The Journal of Experimental Biology 211, 837-843
Published by The Company of Biologists 2008
doi:10.1242/jeb.014340

Quantitative analysis of neonatal skeletal muscle functional improvement in the mouse

David S. Gokhin[1,2], Samuel R. Ward[3], Shannon N. Bremner[1,2] and Richard L. Lieber[1,2,*]

Departments of [1]Bioengineering, [2]Orthopaedic Surgery and [3]Radiology, University of California-San Diego and Veterans Affairs Medical Center, La Jolla, CA 92093, USA

*Author for correspondence (e-mail: rlieber@ucsd.edu)

Accepted 7 January 2008

SUMMARY

Postnatal skeletal muscle growth is classically attributed to fiber hypertrophy and myogenic differentiation, but these processes do not account for the size-independent increase of muscle mechanical performance that occurs during postnatal growth. There is also little knowledge about the precise time-course of contractile function or the underlying factors that affect it. The present study investigated morphological factors (muscle fiber size and myofibrillar packing), biochemical factors (myosin heavy chain isoform and desmin intermediate filament protein expression), and muscle architecture during postnatal development in mice. Physiological testing of the mouse tibialis anterior revealed that maximum isometric stress increased from 27±3 kPa at postnatal day 1 to 169±10 kPa by postnatal day 28, roughly a sixfold increase. Morphological measurements revealed a robust increase in the size-independent packing of myofibrillar matrix material occurring with the functional improvement, with just 48.1±5.5% of the cross-sectional area filled with myofibrils at postnatal day 1 whereas 92.5±0.9% was filled by day 28. Expression of four myosin heavy chain isoforms (embryonic, neonatal, IIX and IIB), as well as desmin, correlated significantly with muscle mechanical function. Stepwise multiple regression showed that, of the variables measured, percentage content of neonatal myosin heavy chain was the best predictor of mechanical function during the postnatal time-course. These data provide the first specific structural basis for increases in muscle tension development during growth. Therefore, models of muscle growth must be modified to include an intrinsic quality enhancement component.

Key words: skeletal muscle, isometric stress, growth, maturation, myofibril, desmin.

INTRODUCTION

Postnatal growth of skeletal muscle in mammals occurs rapidly and continues until adulthood. Rodent studies show that whole-body muscle mass increases 50-fold during growth, and muscle contributes to roughly 50% of added mass of the growing animal (Allen et al., 1979). Postnatal muscle growth is attributed primarily to muscle fiber hypertrophy, which increases the diameter of existing fibers through protein deposition and, synergistically, through the differentiation of myogenic stem cells that synthesize new myotubes and establish new myonuclear domains (Christ and Brand-Saberi, 2002; O'Connor et al., 2007; White and Esser, 1989; Zammit et al., 2006). However, during muscle growth, and specifically during the perinatal period, muscle tissue dramatically increases its mechanical abilities independently of size. In the mouse, muscle isometric stress increases roughly tenfold, from ~25 kPa immediately after birth (Bang et al., 2006) to ~250 kPa by musculoskeletal maturity (Sam et al., 2000). Clearly, a size-independent maturational process occurs during postnatal muscle growth, but the underlying biochemical, morphological and architectural factors that affect function during muscle growth have not been defined.

When considering muscle function, the mechanical machinery may be considered as the composite of the force-generating myofibrillar apparatus and the lateral force transmission network. The principal thick filament constituent of the myofibril is myosin heavy chain (MyHC), and developmental heterogeneity across muscles arises in part from differences in the expression of MyHC isoforms, which include at least two early developmental [embryonic (EMB) and neonatal (NEO)] and four mature (I, IIA, IIX and IIB) isoforms (Bottinelli, 2001; Schiaffino and Reggiani, 1994). Postnatal transitions away from early developmental MyHC isoforms and toward muscle-specific distributions of mature isoforms have been observed in a number of mammalian species (Agbulut et al., 2003; Strbenc et al., 2006; Wank et al., 2006). In the lateral force transmission network, an important constituent is the intermediate filament desmin, which is the first muscle-specific structural protein to be expressed in the embryo (Herrmann et al., 1989; Mayo et al., 1992). Desmin is essential for complete mechanocoupling from the myofibrillar Z-disk to the sarcolemma, and, indirectly, to the extracellular matrix (Li et al., 1997; Sam et al., 2000; Shah et al., 2004). However, it remains unclear whether the maturation of the myofibrillar apparatus or the lateral force transmission network contributes more to the postnatal development of muscle stress.

The purpose of this study was to characterize postnatal skeletal muscle growth in mice during a 4-week postnatal time-course, thereby verifying the hypothesis that skeletal muscle undergoes size-independent functional maturation during growth. The goal was to define the time-courses of tissue morphology (muscle fiber size and packing of myofibrils), muscle architecture, biochemistry of relevant muscle structural proteins (MyHC isoforms and desmin), and size-independent muscle contractile function (maximum isometric stress). Stepwise multiple regression analysis determined the predictive capacity of each growth parameter on contractile function.

MATERIALS AND METHODS

Animals and experimental design

Eight ICR mouse pups (*Mus musculus* Linneaus; Harlan, Indianapolis, IN, USA) were sacrificed on each of five postnatal days 1, 7, 14, 21 and 28 (P1–P28; N=40 mice), yielding 16 hindlimbs/time-point. Mice were sacrificed by halothane inhalation followed by cervical dislocation, except for P1 mice that were sacrificed by decapitation. All procedures were done in accordance to the Institutional Animal Care and Use Committee, UC San Diego and VA Medical Center, San Diego, CA, USA. Both hindlimbs were removed, and the tibialis anterior (TA) muscles were dissected from one of the hindlimbs, snap-frozen in liquid-nitrogen-cooled isopentane, and stored at –80°C for subsequent morphological analysis. The remaining hindlimbs were used for functional analysis (isometric stress and muscle architecture), and the TA muscles were saved for biochemical analysis (SDS–PAGE and western blotting).

Measurement of fiber cross-sectional area

To assess muscle fiber growth, fiber size was measured by laminin immunohistochemistry and image analysis as described previously (Minamoto et al., 2007). Transverse TA sections (thickness: 10 μm) were quenched in methanol:H_2O_2 (3:1) to block endogenous peroxidase activity, and nonspecific binding was blocked with 1% bovine serum albumin (BSA), followed by 1.5% normal goat serum to which 10% normal rat serum was added. Sections were immunolabeled overnight with polyclonal anti-laminin (1:1000; Sigma-Aldrich, St Louis, MO, USA) to label the basement membranes of the muscle cells. Sections were then incubated for 1 h with Alexa Fluor 594-conjugated secondary goat anti-rabbit IgG (Invitrogen, Carlsbad, CA, USA). Sections were preserved in Vectashield mounting medium (Vector Laboratories, Burlingame, CA, USA) and photographed at 10× magnification under a fluorescence microscope. Images were processed in ImageJ (http://rsb.info.nih.gov/ij/; National Institutes of Health, Bethesda, MD, USA) using a custom-made macro that performed image thresholding and computed areas enclosed by 'rings' of pericellular laminin. Filtering criteria were applied to ensure measurement of actual muscle fibers, rejecting regions with cross-sectional areas <50 μm^2 or >5600 μm^2 to eliminate neurovascular structures or 'optically fused' fibers, respectively. In addition, incomplete fibers along the edge of the image were excluded. Finally, regions with circularity (defined as the ratio of the diameters of an ellipse) of <0.3 or >1.0 were excluded to avoid measuring fibers from oblique sections.

Measurement of area fraction of contractile material

Cross-sectional area fraction of contractile material was measured by actin labeling and image analysis. Sections serial to those used for fiber cross-sectional area measurements were fixed in 3.7% formaldehyde and blocked in 1% BSA. Sections were incubated with Alexa Fluor 488-conjugated phalloidin (Invitrogen) to label sarcomeric actin. Sections were preserved in Vectashield and photographed at 40× magnification. Images were thresholded in ImageJ using identical fluorescence intensity cutoff values for all images. The area fraction of fluorescence was used as a measure of the cross-sectional area fraction of contractile material.

Muscle functional assessment

Isometric contractile tests were performed on mouse pup hindlimbs as previously described (Bang et al., 2006). Hindlimbs were transected at the proximal femur, skinned, and immersed in mammalian Ringer solution (137 mmol l^{-1} NaCl, 5 mmol l^{-1} KCl, 24 mmol l^{-1} NaH_2PO_4, 2 mmol l^{-1} $CaCl_2$, 1 mmol l^{-1} $MgSO_4$, 11 mmol l^{-1} glucose and 1 mg l^{-1} curare). Hindlimbs were transferred to a customized muscle-testing chamber filled with Ringer solution (Fig. 1). The fragility of 1-day-old muscle and tendons prevented direct muscle testing, and, therefore, the muscle-tendon–bone complex associated with the TA muscle was used in all experiments. To fix the hindlimb in the chamber, it was secured distal to the TA by tying the ankle to a rigid post interfaced with a force transducer (Model 300B, Aurora Scientific, Aurora, ON, Canada) using silk sutures passing around the tibiotarsal joint space and around the ventral surface of the foot. Proximal to the TA, the sharp end of an anodized stainless steel pin was driven down the shaft of the femur until it protruded from the femoral condyle. The blunt half was secured with a setscrew attached to a rigid frame. The plantarflexors were then released at the Achilles tendon and carefully resected. TA muscle length was measured using a dissecting microscope fitted with an eyepiece crosshair reticule and translating the chamber under the field of view from the TA origin to the myotendinous junction with a digital micrometer. Maximum isometric tension in the dorsiflexors was imposed by applying a 400 ms train of 0.3 ms pulses delivered at 100 Hz while maintaining constant muscle length. This measurement was repeated twice at 2 min intervals. After testing, TA muscles were dissected and weighed. A computer algorithm written in LabVIEW (National Instruments, Austin, TX, USA) performed all data acquisition and analysis of force-time records.

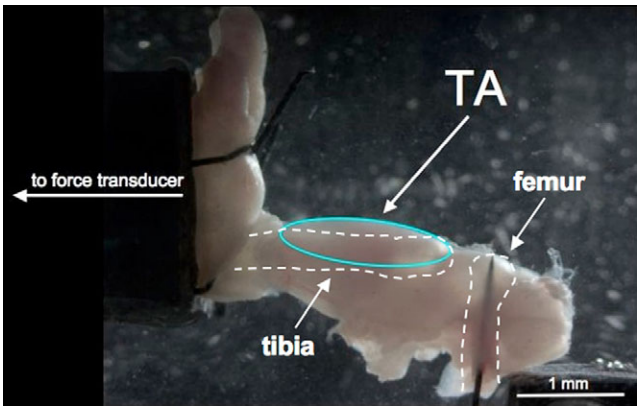

Fig. 1. Photograph of the experimental apparatus for functional testing of mouse pup hindlimbs. In this example, a P1 hindlimb is secured. The tibialis anterior (TA) muscle and the approximate locations of the tibia and femur are indicated.

Muscle architecture and isometric stress calculation

To determine the maximum isometric stress generated by each muscle, isometric tension is typically normalized to physiological cross-sectional area (PCSA), a metric of force-generating capacity (Powell et al., 1984). In this study, an adjusted PCSA* was used to account for variable myofibrillar packing. Muscle mass (M, in mg), muscle density (ρ=1.056, in g cm^{-3}) (Mendez and Keys, 1960), fiber pennation angle (θ=11.7°) (Burkholder et al., 1994), fiber length (L_f, in mm), and the cross-sectional area fraction of contractile material (X_{csa}, as measured previously) were used to compute adjusted PCSA* (in mm^2), using the formula:

$$PCSA^* = (M\cos\theta/\rho L_f) \times X_{csa} . \quad (1)$$

L_f was determined for each specimen using a TA fiber:muscle length ratio of 0.6, which was obtained in a pilot experiment using 10

formalin-fixed neonatal TA muscles. This neonatal TA fiber:muscle length ratio agreed with the adult value determined previously (Burkholder et al., 1994). Analysis of muscle stress instead of force allowed comparison of intrinsic muscle contractility independent of muscle size.

Validation of muscle functional assessment

A pilot experiment was performed in which dorsiflexors from adult mice were isometrically tested either without (N=4) or with (N=4) transection of the tibia to eliminate ankle joint torque. Isometric stresses in both groups were statistically indistinguishable (203±10 kPa without transection, 227±20 kPa with transection; P>0.1), indicating that force redirection due to ankle rotation did not occur in the experimental apparatus. In addition, laser diffraction was to used to measure sarcomere length in 12 mouse TA muscles, each formalin-fixed at a 90° ankle angle, which was identical to the ankle angle at which TA muscles were tested in the experimental apparatus (Fig. 1). The sarcomere length was 2.32±0.08 μm, indicating that functional experiments were performed near the plateau of the length-tension curve of the TA.

Gel electrophoresis of myosin heavy chain isoforms

MyHC isoform distributions were determined by adapting the gel electrophoresis technique previously described (Talmadge and Roy, 1993). Muscles were homogenized, and the myofibril-rich pellet was washed and resuspended in buffer supplemented with protease cocktail (5 μl of 100 mmol l^{-1} PMSF, 10 μg μl^{-1} leupeptin and 10 μg μl^{-1} pepstatin A). Protein was then diluted in sample buffer to a concentration of 0.125 mg ml^{-1} across all muscle homogenates regardless of initial muscle size. Separation of MyHC isoforms was performed with SDS–PAGE on polyacrylamide gels (16 cm×22 cm, thickness: 0.75 mm) for 22 h of migration at 275 V at 4°C. Stacking and resolving gels were 4% and 8% polyacrylamide, respectively. After migration, gels were silver stained according to the manufacturer's instructions (Bio-Rad, Hercules, CA, USA). The positions of MyHC isoforms were determined by their relative electrophoretic mobilities, which have been characterized previously (Agbulut et al., 2003; Schiaffino et al., 1989). Densitometry was performed to compute band intensities (Quantity One, Bio-Rad) and resultant MyHC isoform distributions.

Western blotting for desmin

The muscle homogenates were separated with SDS–PAGE on 14% polyacrylamide gels with 2.5 h of migration at 20 mA at 4°C. Exogenous desmin standards (1–10 ng μl^{-1}; Fitzgerald Industries International, Concord, MA, USA) were included for quantification of unknown samples. Homogenates were transferred onto nitrocellulose membranes for 1 h at 100 V at 4°C. Following 1 h of blocking in 5% nonfat milk, membranes were incubated overnight in monoclonal anti-desmin (DER11; Vision BioSystems, Norwell, MA, USA), and then incubated for 1 h in horseradish peroxidase-conjugated secondary anti-mouse IgG (Vector Laboratories). Bands were detected using enhanced chemiluminescence according to the manufacturer's instructions (ECL, GE Healthcare Biosciences, Piscataway, NJ, USA) followed by densitometry.

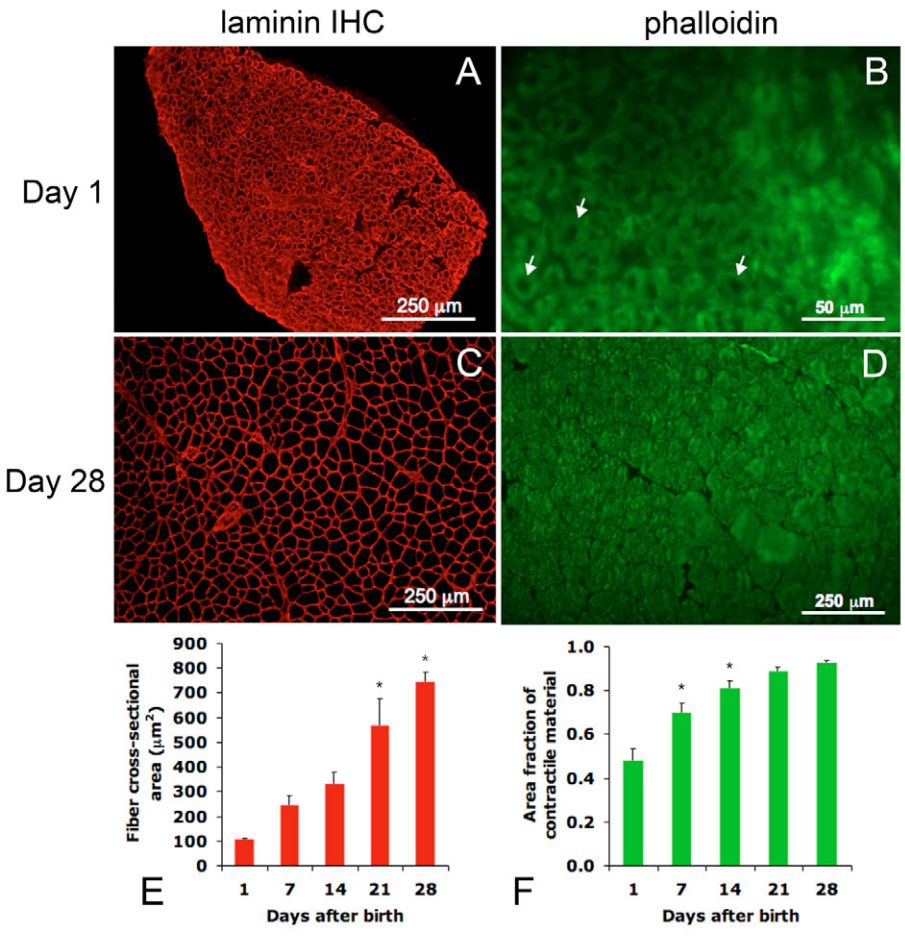

Fig. 2. Fluorescence microscopy of transverse tibialis anterior (TA) muscle sections at P1 (A,B) and P28 (C,D) using laminin immunohistochemistry for muscle fiber size measurement (A,C) and phalloidin staining for measurement of myofibrillar packing (B,D). Extensive muscle hypertrophy and accumulation of myofibrillar material is evident between P1 and P28. Arrows in B indicate examples of how immature muscle fibers typically begin to accumulate myofibrillar material first in the subsarcolemmal region and then inward toward the central axis of the cell. Image B is shown at a higher magnification for clarity. Postnatal time-courses of fiber size (E) and the fraction of the cross-sectional area occupied by contractile material (F) are also presented. *P<0.05 relative to the previous time-point.

Statistics

The effect of postnatal day on morphological, functional and biochemical parameters was assessed by one-way analysis of variance (ANOVA) with *post-hoc* Fisher's PLSD comparisons. For architectural or biochemical parameters, linear regression was used to analyze relationships between those parameters and isometric stress. To determine the relative contributions of each parameter, the data were reanalyzed with stepwise multiple regression. A P value of <0.05 was considered statistically significant, and data are presented as mean ± standard error (s.e.m.).

RESULTS

Animal mass increased from 1.9±0.1 gm at P1 to 22.2±0.8 g at P28 (Fig. 3A), consistent with vendor-supplied growth data. Pups engaged in adult patterns of locomotor activity by P21, at which point they were weaned from their mothers.

Muscle morphology exhibited rapid postnatal maturation. At P1, muscle fiber cross-sectional area was low (107±3 μm^2; Fig. 2A), indicating little or no effect of hypertrophy on fiber size at this early time-point. Fiber cross-sectional area increased approx. sevenfold from P1 to P28 (Fig. 2E), and, by P28, fiber cross-sectional area had risen to 745±40 μm^2 (Fig. 2C), which is closer to, but still below, the adult fiber cross-sectional area of ~1000 μm^2 (Barash et al., 2007; Hamalainen and Pette, 1993; Sartorius et al., 1998). Strikingly, the packing of myofibrils was very low at P1, with only 48.1±5.5% of the cross-sectional area occupied by contractile material (Fig. 2B). In incompletely filled fibers, accumulation of myofibrils began in the subsarcolemmal region and moved inward, resulting in the appearance of 'hollow' muscle fibers lacking contractile material near their central axes (Fig. 2B). Myofibrillar packing at P28 had reached approximately adult levels, with 92.5±0.9% of the cross-sectional area filled by myofibrils (Fig. 2D). Such a robust increase in myofibrillar packing indicated a near-total filling of the intracellular space by contractile protein by P28 (Fig. 2F).

Morphological maturation occurred synchronously with functional enhancement. The maximum isometric force generated by successive isometric contractions deviated by less than 1%, indicating that hindlimbs did not loosen from the testing apparatus or experience fatigue effects (data not shown). Maximum isometric force increased by approx. fivefold during the experimental time-course, from 1.7±0.1 g at P1 to 8.5±0.4 g by P28. However, since force increase largely arose from an increase in muscle size, *stress* was preferred as the metric for intrinsic mechanical function. Isometric stress exhibited an approx. sixfold increase from 27±3 kPa at P1 to 169±10 kPa by P28 (Fig. 3E), defining the size-independent increase in mechanical quality during postnatal growth.

Certain architectural parameters followed growth time-courses similar to the morphological parameters and correlated well with isometric stress. For example, muscle mass increased an approx. fourfold from P1 to P28 (Fig. 3B). Similarly, L_f increased approx. fivefold across the experimental time-course (Fig. 3C). Muscle PCSA* did not increase as vigorously, as indicated by a 50% increase from P1 to P28 (Fig. 3D). By ungrouping the samples from postnatal day, it was revealed that both muscle mass ($P<0.001$; Fig. 3F) and L_f ($P<0.0001$; Fig. 3G) exhibited significant positive correlations with isometric stress. On the other hand, PCSA* exhibited no significant correlation with isometric stress ($P>0.1$, Fig. 3H). Both muscle mass and L_f served as proxies for animal age, so their significant correlations with stress were not surprising.

As expected (Agbulut et al., 2003; Strbenc et al., 2006), postnatal levels of MyHC isoforms EMB and NEO declined to 0% while expression of isoforms IIX and IIB increased to approximately adult

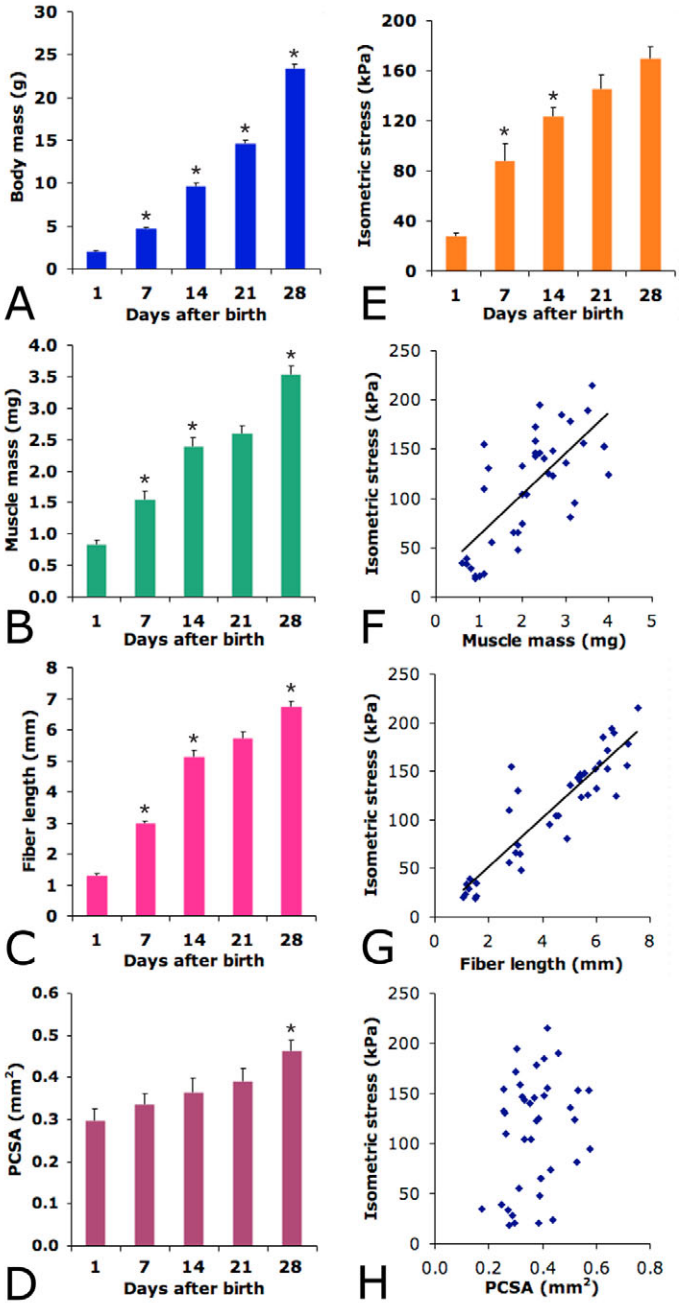

Fig. 3. Postnatal time-course of whole body mass (A), three architectural parameters: muscle mass (B), fiber length (C) and physiological cross-sectional area (PCSA; D), and postnatal time-course of isometric stress (E). Muscle mass (F) and fiber length (G) were positively correlated with contractile function (mass: $P<0.001$, $R^2=0.52$; fiber length: $P<0.0001$, $R^2=0.82$), but PCSA (H) was uncorrelated ($P>0.1$, $R^2=0.06$). *$P<0.05$ relative to the previous time-point.

values (33.7±3.4% IIX and 63.0±1.2% IIB) by P28 (Fig. 4A). Maximum isometric stress was negatively correlated with levels of EMB and NEO ($P<0.001$ for each; Fig. 4B,C) but positively correlated with levels of IIX and IIB ($P<0.001$ for each; Fig. 4F,G). That both IIX and IIB isoforms were predictors of contractile function was of particular interest because they are the principal thick filament constituents of the mature mouse TA. Low levels of isoforms I and IIA were observed but did not correlate with

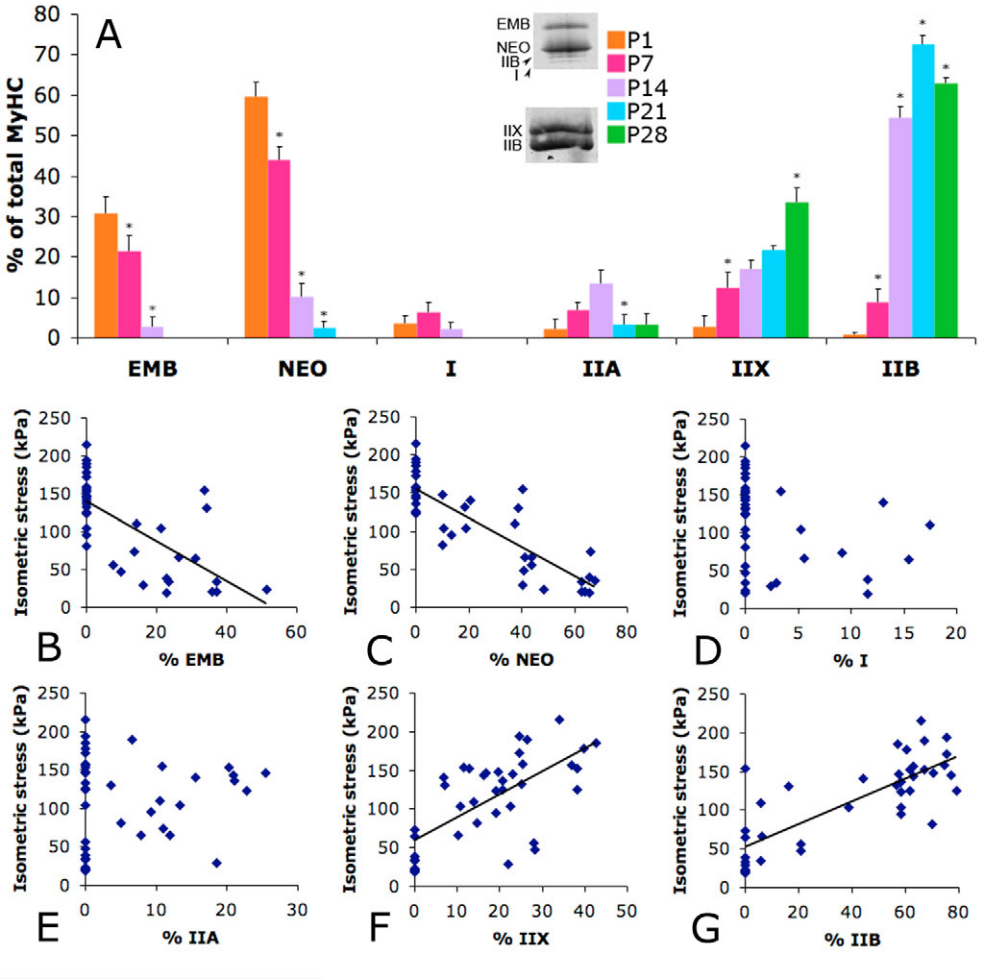

Fig. 4. Postnatal time-course of expression of MyHC isoforms (A) and the influence of individual MyHC isoforms on isometric stress (B–G). Sample MyHC gels of P1 and P28 muscle are shown next to the legend in A. The embryonic (EMB), neonatal (NEO), and IIX and IIB mature isoforms were all significantly correlated with contractile function (P<0.001 for each, R^2_{EMB}=0.48, R^2_{NEO}=0.72, R^2_{IIX}=0.46, R^2_{IIB}=0.62), although NEO was the strongest predictor as determined by stepwise multiple regression. Neither isoform I nor IIA was significantly correlated with contractile function (P>0.05 for each, R^2_{I}=0.09, R^2_{IIA}=0.01). *P<0.05 relative to the previous time-point.

contractile function (P>0.05 for each; Fig. 4D,E), which is appropriate given that neither I nor IIA are substantially present in the mature mouse TA. Desmin levels increased immediately postnatally but quickly plateaued by P7 (Fig. 5A), indicating that adult levels of desmin were achieved before that time-point. Desmin levels exhibited a weak but statistically significant correlation with isometric stress (P<0.05; Fig. 5B). These regressions indicate that MyHC composition explained more of the variance in isometric stress than desmin.

Stepwise multiple regression analysis was used to determine which architectural and/or biochemical parameter(s) were the best predictors of isometric stress. Using a critical F-to-enter of 4, three regression steps were necessary: (1) the first step of the multiple regression identified L_f as the strongest predictor of isometric stress (F-to-enter=171.8); (2) the second step identified PCSA (F-to-enter=8.9); and (3) the third step identified EMB (F-to-enter=6.3). Because architectural variables depend on muscle size, stepwise regression was performed again using only biochemical parameters. This time, one regression step was necessary because the first step identified NEO as the strongest predictor of isometric stress (F-to-enter=99.8). Together, these data indicate that the decline in early developmental MyHC isoforms was the best size-independent predictor of isometric stress. However, none of these variables are entirely 'independent' and probably co-vary during development.

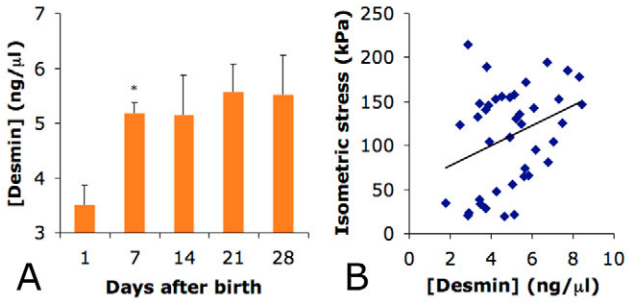

Fig. 5. Time-course of desmin levels postnatally (A) and its influence on isometric stress (B). Desmin levels were weakly but significantly correlated with contractile function (P<0.05, R^2=0.11). *P<0.05 relative to the previous time-point.

DISCUSSION

The age-dependent increase in isometric stress offers the first direct demonstration of the improvement of functional quality during the postnatal development of skeletal muscle. Although the architectural variables observed here did correlate with stress, they all served as various proxies for 'size' and did not reveal underlying cellular processes that would explain the improvement in function. Considering the morphological data, the rise in stress is most likely due to an increase in myofibrillar packing rather than an increase in fiber size. Fiber hypertrophy causes increases in muscle *force*, but a marker of muscle maturation is needed to account for the increased muscle *stress*. An increase in the packing of myofibrils, however, is a size-independent observation that results in enhanced force generation per unit cross-sectional area. The low (~48%) filling

of P1 muscle, compared to the near-total (~92%) filling of P28 muscle, is one basis for the severely impaired stress-generation capacity of newborn mouse muscle.

In this study, the isometric stress observed at P28 (~170 kPa) is still considerably less than the isometric stress of ~250 kPa observed in mature mouse muscles (Sam et al., 2000). Assuming that functional quality continues to improve into weeks beyond the terminal 4-week time-point used in this study, it may be useful to locate the time-point when mature stress generation is achieved. While 4 postnatal weeks is sufficient for skeletal maturity, additional time is necessary for muscular maturity, and the age at which mouse muscles can generate ~250 kPa of isometric stress may define true musculoskeletal maturity.

Because the fragility and small size of neonatal muscles prevented direct isometric testing, whole-hindlimb preparations were used instead to measure tetanic forces in the dorsiflexors. This system is prone to several sources of error, especially in the PCSA calculation in Eqn 1. For example, forces were normalized to the PCSA of the TA muscle alone and neglected the cross-sectional area contributions of the other ankle dorsiflexors, such as the extensor digitorum longus (EDL) and extensor hallucis longus (EHL). Therefore, the PCSAs used here were systematically too low, resulting in stress values that were systematically high. A previous architectural study in adult mice (Burkholder et al., 1994) has shown that the PCSAs of the EDL (1.8±1.6 cm^2) and EHL (0.2±0.1 cm^2) relative to the TA (5.3±0.6 cm^2) occupy ~27% of the cross-sectional area of the dorsiflexion musculature, suggesting that the impact of this effect is significant but difficult to quantify without knowledge of the relative muscle PCSAs in neonatal mice. In addition, PCSA calculations assumed constant muscle density regardless of age. This assumption is imperfect, especially since the morphological data showed enhanced myofibrillar packing that might result in an age-dependent increase in muscle density. However, the error produced by this assumption is probably small, since mature mouse muscle density (1.056 g cm^{-3}) is very close to that of water, and the myofibril-free volume fraction of immature muscle tissue contains mostly water.

Interestingly, early developmental isoforms of MyHC (EMB and NEO) were the strongest predictors of isometric stress as determined by the stepwise regression analysis, which is reasonable considering that their dramatic postnatal reductions occur almost exactly during the 4-week experimental time-course used here. However, this result is strictly correlative and does not suggest a causal relationship between reduced EMB or NEO expression and enhanced mechanical function. Rather, the progressive displacement of EMB and NEO by mature isoforms IIX and IIB is a more likely cause, with early developmental isoforms playing placeholder roles for mature isoforms during development. Gradual reconstruction of the thick filament occurs during developmental remodeling of muscle through a process mediated by thyroid hormone, probably resulting in the transient existence of hybrid thick filaments (Butler-Browne and Whalen, 1984; Butler-Browne et al., 1987; Adams et al., 1999). The biomechanical effects of thick filament reconstruction and MyHC isoform heterogeneity during development remain unknown.

Western blotting for desmin indicated that the lateral force transmission network contributes to the postnatal enhancement of contractile function but not as robustly as MyHC. Therefore, it is likely that the lateral force transmission network is secondary to the myofibrillar apparatus in the postnatal development of muscle stress. While age-dependent changes in desmin levels were less striking than the maturation of MyHC, the western blots used here were limited in that they could not detect possible maturation of desmin cytoskeletal architecture (e.g. enhanced attachment to costameres and/or myofibrillar Z-disks). It is also likely that maturation occurs in other muscle-specific but non-myofibrillar molecular systems that were not explored in this study, such as neuromuscular junction specification, calcium handling and costamere assembly. Maturation of these systems would result in improved muscle contractility independent of either the myofibrillar apparatus or the lateral force transmission network.

The mechanical, morphological and biochemical data all support the notion of size-independent increases in muscle contractile function during growth. Therefore, the bipartite model of muscle growth, incorporating fiber hypertrophy and myogenic differentiation, is incomplete. A third aspect – intrinsic functional enhancement – needs to be considered as well. Together, these aspects of muscle growth may define a three-dimensional 'growth space' through which muscles pass during their progression from immature to mature stages of postnatal development. It is likely that muscles follow distinct trajectories through the growth space depending on their anatomical geometries and functional demands. The growth space trajectory of a muscle may serve as a type of developmental fingerprint for its native function.

The structural and functional data regarding neonatal skeletal muscle presented here provide a secondary benefit to investigators researching the physiology of muscle-specific proteins. Specifically, these data are necessary to serve as a reference for studying certain muscle-specific proteins whose knockout is neonatal-lethal in mouse models. Examples of such proteins include Myf5, a transcription factor mediating myogenic commitment (Braun et al., 1992), nebulin, a regulator of thin filament assembly (Bang et al., 2006; Witt et al., 2006), and Cypher, a Z-disk stabilizer (Zhou et al., 2001). In these models, severe postnatal myofibrillar degeneration and muscle fiber necrosis occur secondarily to the gene deletion and render invalid any comparison with age-matched or mature wild-type controls. Therefore, comparison with immature wild-type controls at neonatal time-points is preferred.

We gratefully acknowledge the National Institutes of Health grant AR40050 and the Department of Veterans Affairs. We also thank Amanda Felder for generating the sarcomere length *versus* joint angle data for the validation study.

REFERENCES

Adams, G. R., McCue, S. A., Zeng, M. and Baldwin, K. M. (1999). Time course of myosin heavy chain transitions in neonatal rats: importance of innervation and thyroid state. *Am. J. Physiol.* **276**, R954-R961.

Agbulut, O., Noirez, P., Beaumont, F. and Butler-Browne, G. (2003). Myosin heavy chain isoforms in postnatal muscle development of mice. *Biol. Cell* **95**, 399-406.

Allen, R. E., Merkel, R. A. and Young, R. B. (1979). Cellular aspects of muscle growth: myogenic cell proliferation. *J. Anim. Sci.* **49**, 115-127.

Bang, M. L., Li, X., Littlefield, R., Bremner, S., Thor, A., Knowlton, K. U., Lieber, R. L. and Chen, J. (2006). Nebulin-deficient mice exhibit shorter thin filament lengths and reduced contractile function in skeletal muscle. *J. Cell Biol.* **173**, 905-916.

Barash, I. A., Bang, M. L., Mathew, L., Greaser, M. L., Chen, J. and Lieber, R. L. (2007). Structural and regulatory roles of muscle ankyrin repeat protein family in skeletal muscle. *Am. J. Physiol.* **293**, C218-C227.

Bottinelli, R. (2001). Functional heterogeneity of mammalian single muscle fibres: do myosin isoforms tell the whole story? *Pflugers Arch.* **443**, 6-17.

Braun, T., Rudnicki, M. A., Arnold, H. H. and Jaenisch, R. (1992). Targeted inactivation of the muscle regulatory gene Myf-5 results in abnormal rib development and perinatal death. *Cell* **71**, 369-382.

Burkholder, T. J., Fingado, B., Baron, S. and Lieber, R. L. (1994). Relationship between muscle fiber types and sizes and muscle architectural properties in the mouse hindlimb. *J. Morphol.* **221**, 177-190.

Butler-Browne, G. S. and Whalen, R. G. (1984). Myosin isozyme transitions occurring during the postnatal development of the rat soleus muscle. *Dev. Biol.* **102**, 324-334.

Butler-Browne, G. S., Pruliere, G., Cambon, N. and Whalen, R. G. (1987). Influence of the dwarf mouse mutation on skeletal and cardiac myosin isoforms. Effect of one injection of thyroxine on skeletal and cardiac muscle phenotype. *J. Biol. Chem.* **259**, 15188-15193.

Christ, B. and Brand-Saberi, B. (2002). Limb muscle development. *Int. J. Dev. Biol.* **46**, 905-914.

Hamalainen, N. and Pette, D. (1993). The histochemical profiles of fast fiber types IIB, IID, and IIA in skeletal muscles of mouse, rat, and rabbit. *J. Histochem. Cytochem.* **41**, 733-743.

Herrmann, H., Fouquet, B. and Franke, W. W. (1989). Expression of intermediate filament proteins during development of *Xenopus laevis*. II. Identification and molecular characterization of desmin. *Development* **105**, 299-307.
Li, Z., Mericskay, M., Agbulut, O., Butler-Browne, G., Carlsson, L., Thornell, L. E., Babinet, C. and Paulin, D. (1997). Desmin is essential for the tensile strength and integrity of myofibrils but not for myogenic commitment, differentiation, and fusion of skeletal muscle. *J. Cell Biol.* **139**, 129-144.
Mayo, M. L., Bringas, P., Jr, Santos, V., Shum, L. and Slavkin, H. C. (1992). Desmin expression during early mouse tongue morphogenesis. *Int. J. Dev. Biol.* **36**, 255-263.
Mendez, J. and Keys, A. (1960). Density and composition of mammalian muscle. *Metabolism* **9**, 184-188.
Minamoto, V. B., Hulst, J. B., Lim, M., Peace, W. J., Bremner, S. N., Ward, S. R. and Lieber, R. L. (2007). Increased efficacy and decreased systemic-effects of botulinum toxin A injection after active or passive muscle manipulation. *Dev. Med. Child Neurol.* **49**, 907-914.
O'Connor, R. S., Pavlath, G. K., McCarthy, J. J. and Esser, K. A. (2007). Point:Counterpoint: satellite cell addition is/is not obligatory for skeletal muscle hypertrophy. *J. Appl. Physiol.* **103**, 1099-1102.
Powell, P. L., Roy, R. R., Kanim, P., Bello, M. A. and Edgerton, V. R. (1984). Predictability of skeletal muscle tension from architectural determinations in guinea pig hindlimbs. *J. Appl. Physiol.* **57**, 1715-1721.
Sam, M., Shah, S., Friden, J., Milner, D. J., Capetanaki, Y. and Lieber, R. L. (2000). Desmin knockout muscles generate lower stress and are less vulnerable to injury compared with wild-type muscles. *Am. J. Physiol.* **279**, C1116-C1122.
Sartorius, C. A., Lu, B. D., Acakpo-Satchivi, L., Jacobsen, R. P., Byrnes, W. C. and Leinwand, L. A. (1998). Myosin heavy chains IIa and IId are functionally distinct in the mouse. *J. Cell Biol.* **141**, 943-953.
Schiaffino, S. and Reggiani, C. (1994). Myosin isoforms in mammalian skeletal muscle. *J. Appl. Physiol.* **77**, 493-501.
Schiaffino, S., Gorza, L., Sartore, S., Saggin, L., Ausoni, S., Vianello, M., Gundersen, K. and Lomo, T. (1989). Three myosin heavy chain isoforms in type 2 skeletal muscle fibres. *J. Muscle Res. Cell Motil.* **10**, 197-205.
Shah, S. B., Davis, J., Weisleder, N., Kostavassili, I., McCulloch, A. D., Ralston, E., Capetanaki, Y. and Lieber, R. L. (2004). Structural and functional roles of desmin in mouse skeletal muscle during passive deformation. *Biophys. J.* **86**, 2993-3008.
Strbenc, M., Smerdu, V., Pogacnik, A. and Fazarinc, G. (2006). Myosin heavy chain isoform transitions in canine skeletal muscles during postnatal growth. *J. Anat.* **209**, 149-163.
Talmadge, R. J. and Roy, R. R. (1993). Electrophoretic separation of rat skeletal muscle myosin heavy-chain isoforms. *J. Appl. Physiol.* **75**, 2337-2340.
Wank, V., Fischer, M. S., Walter, B. and Bauer, R. (2006). Muscle growth and fiber type composition in hind limb muscles during postnatal development in pigs. *Cells Tissues Organs* **182**, 171-181.
White, T. P. and Esser, K. A. (1989). Satellite cell and growth factor involvement in skeletal muscle growth. *Med. Sci. Sports Exerc.* **21**, S158-S163.
Witt, C. C., Burkart, C., Labeit, D., McNabb, M., Wu, Y., Granzier, H. and Labeit, S. (2006). Nebulin regulates thin filament length, contractility, and Z-disk structure *in vivo*. *EMBO J.* **25**, 3843-3855.
Zammit, P. S., Partridge, T. A. and Yablonka-Reuveni, Z. (2006). The skeletal muscle satellite cell: the stem cell that came in from the cold. *J. Histochem. Cytochem.* **54**, 1177-1191.
Zhou, Q., Chu, P. H., Huang, C., Cheng, C. F., Martone, M. E., Knoll, G., Shelton, G. D., Evans, S. and Chen, J. (2001). Ablation of Cypher, a PDZ-LIM domain Z-line protein, causes a severe form of congenital myopathy. *J. Cell Biol.* **155**, 605-612.